CRYSTAL GROWTH & DESIGN

Article

pubs.acs.org/crystal

# Atmospheric Pressure Cold Plasma Synthesis of Submicrometer-Sized Pharmaceuticals with Improved Physicochemical Properties

*Published as part of the Crystal Growth & Design virtual special issue of selected papers presented at the 10th International Workshop on the Crystal Growth of Organic Materials (CGOM10)*

Norbert Radacsi,*[,†] Rita Ambrus,[‡] Piroska Szabó-Révész,[‡] Antoine van der Heijden,[†,§] and Joop H. ter Horst[†]

[†]Process & Energy Laboratory, Delft University of Technology, Leeghwaterstraat 44, 2628 CA Delft, The Netherlands

[‡]Department of Pharmaceutical Technology, University of Szeged, Eötvös street 6, H-6720 Szeged, Hungary

[§]Technical Sciences, TNO, 2280 AA Rijswijk, The Netherlands

Supporting Information

**ABSTRACT:** A reduction in particle size is one of the strategies to enhance the dissolution behavior of low water-soluble drugs such as niflumic acid. Atmospheric pressure cold plasma crystallization is a novel technique to achieve such submicrometer particles. This technique uses a surface dielectric barrier discharge (SDBD) plasma that both charges and heats solution droplets. Atmospheric pressure cold plasma crystallization was used to produce niflumic acid crystals and its excipient, Poloxamer 188, with a significant decrease in size compared to the conventional products. A substantial increase in dissolution rate of the submicrometer niflumic acid was observed in the presence of the plasma-made excipient.

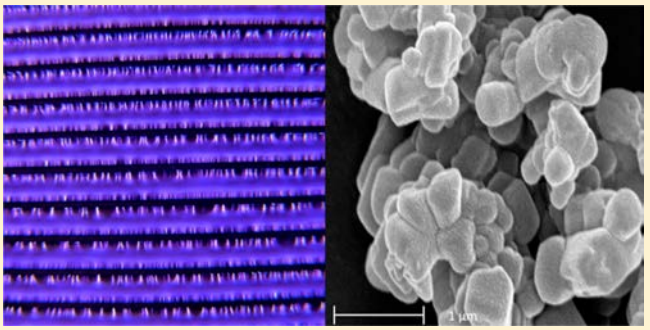

## INTRODUCTION

Solving bioavailability problems of new active pharmaceutical ingredients is a major challenge for the pharmaceutical industry, since nearly half of the new active substances in the pipeline are either insoluble or poorly soluble in water.[1−3] Studies with poorly water-soluble drugs have demonstrated that particle size reduction to the submicrometer range can lead to an increase in the dissolution rate (the total amount of drug substance that dissolves per unit time) and a higher bioavailability.[4−7]

By decreasing the crystal product size, the surface-to-volume ratio is increased. Due to the relatively larger surface area, the dissolution rate is enhanced so that a higher concentration can be reached in shorter time frames. Since, according to the Ostwald−Freundlich relation, smaller particles have increased solubility,[8] an increase in the solubility might be expected as well, possibly further increasing the dissolution rate. Thus, a substantial particle size reduction can offer a solution for bioavailability problems of a specific drug.

There are several techniques to produce nanoparticles. The nanosuspension engineering processes currently used are pearl milling and high-pressure homogenization, either in water or in mixtures of water and water-miscible liquids or nonaqueous media.[9−13] However, milling changes the crystal shape and often results in formation of (partially) amorphous materials because of the high energy input.[14] High pressure homogenization can also produce amorphous materials and sometimes causes decomposition of the crystals, again because of the relatively high energy input. A more advanced method is electrospray crystallization,[15] but the low production rate is a limiting factor. Cold plasma technology offers the possibility to produce a wide range of nanoparticles and to coat them in the same process or to change their hydrophobic properties to hydrophilic or to increase their mechanical stability.[16] Plasma processing is relatively inexpensive, energy efficient, and easily scalable to industrial levels.[17] Furthermore, plasma processes are considered as an environmentally benign technology.[18]

Niflumic acid (NIF) is an important anti-inflammatory drug with a weak analgesic effect.[19] It is primarily used to treat different forms of rheumatism, such as rheumatoid arthritis or arthrosis.[20] However, its poor aqueous solubility[21] and dissolution rate[22] are disadvantages. To achieve optimal pharmacodynamic properties such as a rapid onset of the drug effect, fast dissolution is critical. In practice, certain excipients, such as Poloxamer 188, are added to NIF, the crystalline product, to improve its physical and chemical properties.

The aim of this study is to prepare submicrometer-sized crystals of NIF as well as of its excipient Poloxamer 188 in

**Received:** July 20, 2012
**Revised:** August 31, 2012
**Published:** September 7, 2012





dx.doi.org/10.1021/cg301026b | *Cryst. Growth Des.* 2012, 12, 5090−5095

order to achieve fast dissolution and rapid onset of the drug effect. Atmospheric pressure cold plasma crystallization is introduced as a potential method for the production of submicrometer-sized drug crystals with the possibility of scaling up the process. The differences in dissolution rate as well as the product morphology and crystal form of the produced crystals are also investigated.

## EXPERIMENTAL SECTION

**Materials.** *Niflumic acid* (2-[[3-(trifluoromethyl)phenyl]amino]-3-pyridinecarboxylic acid, see Figure 1 for molecular structure) with a median particle size of around 80 $\mu$m (see Figure S1 for the SEM images of the original product (Supporting Information)) was purchased from Sigma-Aldrich, USA. *β-D-Mannitol* with a median particle size of around 86 $\mu$m was purchased from Hungaropharma Plc., Hungary, and *Poloxamer 188* (polyethylene-polypropylene glycol, see Figure 1 for molecular structure) with a median particle size of around 122 $\mu$m was purchased from Fluka, Slovenia. For the plasma crystallization process, different solution concentrations were prepared with 99.8% acetone purchased from Merck.

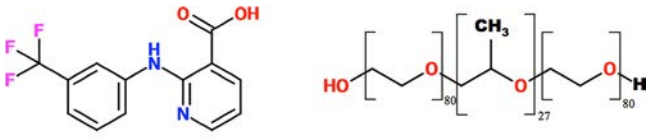


**Figure 1.** Molecular structure of niflumic acid and Poloxamer 188.

**Plasma Crystallization Setup.** Surface dielectric barrier discharge (SDBD) plasma crystallization is a new technique for the synthesis of organic submicrometer-sized crystals. SDBD is a type of cold plasma that can be operated at atmospheric pressure. The plasma is generated on top of the surface of an SDBD plate. The plate is made of 96% alumina ceramics ($Al_2O_3$) and is 1 mm in thickness. An electrode system is deposited onto the SDBD plate. There are discharge electrodes on one side that consist of line-shaped conductors that are deposited on or are partly embedded in the dielectric material. This electrode system consists of 20 interconnected 1 mm wide, 80 mm long, and 50 $\mu$m thick strips of platinum deposited on the ceramic plate. The gap between the electrode strips is 3 mm. A plate-shaped counter-electrode is embedded in the dielectric on the opposite side of the plate (Figure 2). This configuration results in a strong electric field close to the discharge electrodes. The plasma then is a result of discharges caused by a pulsed high voltage between the discharge- and the counter-electrodes.[23] A Xantrex XFR 600-4 DC power supply connected to a homemade AC power supply and a BNC 565 pulse/delay generator was used to create the pulsed AC voltage.

Argon gas at 2 bar pressure was transported through a Collison nebulizer (BGI Inc., USA) and carried the solution as an aerosol spray into the plasma chamber. A Sierra Smart-Track flow meter was used to control the argon flow rate. In order to direct the entire aerosol above the plasma, a stainless steel nozzle was used with an 8 mm slit (Figure 2). The length of the nozzle is 70 mm. Two strong neodymium magnets held the nozzle in place and made it easy to remove. By applying a DC bias voltage superposed on the AC voltage, the plasma can be used as a charger and the uniformly charged particles can be collected on the grounded plasma reactor chamber wall (Figure 2). To use the plasma as a charger, an additional DC power supply (Spellman SL1200 +10 kV, USA) was added to the setup, which was connected between the SDBD plate electrodes with a 5 MΩ resistor.

**Equipment for Electrical and Thermal Measurements.** The high voltage was measured by a Tektronix P6015A high voltage probe, and the current was measured by a Pearson 2877 current monitor. Both were connected to a LeCroy WaveSurfer 44Xs oscilloscope. A Neoptix ReFlex 4-channel fiber optic temperature thermometer (Neolink, USA) was used to measure the temperature surrounding the plasma with a PTFE-coated Neoptix T1 optical temperature probe. The optical sensor was placed 8 mm above the center of the SDBD plate during the experiments. The step-response time of the system was 250 ms.

**Characterization of the Product.** Scanning electron microscopy (SEM) was used to investigate the particles with a Hitachi S4700 electron microscope (Hitachi Scientific Ltd., Japan). A sputter coating apparatus (Bio-Rad SC 502, VG Microtech, England) was applied to induce electric conductivity on the surface of the samples. The air pressure was 1.3−13.0 mPa. NIF particle diameter distributions were obtained by analyzing several SEM images with the ImageJ software environment.[24,25] Over 150 individual particle measurements were made in at least five different images in order to determine the particle size distribution.

X-ray powder diffraction (XRPD) was carried out in order to determine the crystalline form of the produced materials. Samples were measured with a Bruker D8 Advance diffractometer (Bruker AXS GmbH, Karlsruhe, Germany). Data collection was carried out at room temperature using monochromatic Cu K$\alpha$1 radiation ($\alpha$ = 0.154060 nm) in the 2$\theta$ region between 3° and 50°, with a step size of 0.02 deg 2$\theta$. Data evaluation was done with the Bruker program EVA.

Differential scanning calorimetry (DSC) was employed to investigate the melting behavior of the NIF samples. The Mettler Toledo thermal analysis system with the STAR$^e$ thermal analysis program V9.1 (Mettler Inc., Schwerzenbach, Switzerland) was applied to characterize the thermal behavior of the products. The DSC measurements were done with 2−5 mg of NIF in the temperature range between 25 and 300 °C. The heating rate was 5 °C min$^{-1}$. Argon was used as carrier gas at a flow rate of 10 L h$^{-1}$ during the DSC investigation.

FT-IR spectroscopy was used to investigate the chemical stability of the drug. FT-IR spectra were measured on an AVATAR 330 FT-IR apparatus (Thermo Nicolet, USA), in the interval 400−4000 cm$^{-1}$, at 4 cm$^{-1}$ optical resolution. Standard KBr pellets were prepared from 150 mg of KBr pressed with 10 ton and the calculated amount of the samples containing 0.5 mg of NIF.

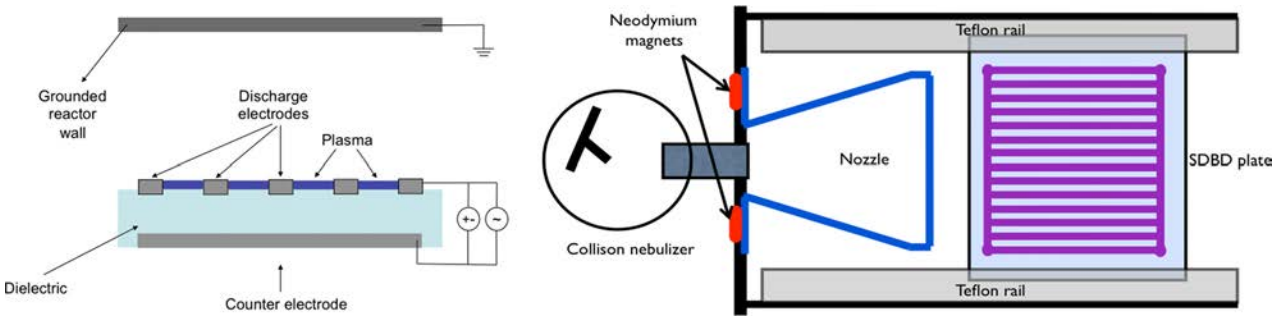


**Figure 2.** Left: Schematic cross section of an SDBD plate with the grounded reactor wall above, which was used for electrostatic collection of the charged particles. Right: The schematic representation of the SDBD plasma reactor with the nozzle and the SDBD plate.


dx.doi.org/10.1021/cg301026b | Cryst. Growth Des. 2012, 12, 5090−5095

**Dissolution Rate Measurements.** The dissolution of different powder samples, containing the same amount of drug (14 mg according to the dose), was determined according to the paddle method.[26] A phosphate buffer solution (50 mL, pH 1.2 ± 0.1) at 37 ± 0.5 °C was used as a dissolution medium, and the rotation speed of the paddles was set at 100 rpm. At certain time intervals, 2 mL solution samples were withdrawn and filtered (cutoff 0.2 μm, Minisart SRP 25, Sartorius, Germany), and the amount of dissolved drug was determined by an ATI-Unicam UV2-100 UV/vis spectrophotometer. The withdrawn samples were replaced by fresh medium, as is done in common practice. The dissolution behavior was determined in the presence and absence of excipients, both for conventional and submicrometer-sized NIF. D-Mannitol and Poloxamer 188 were used as excipients to help the deaggregation and increase the wettability of the NIF crystals. D-Mannitol acts as a carrier, which provides the homogeneous distribution of the NIF crystals, while Poloxamer 188 helps as a stabilizer by wetting the particles to minimize (or inhibit) the aggregation of the drug.[27] Table 1 shows the ratio of the excipients added to the drug. The physical mixtures were prepared using a Turbula mixer for 10 min, as suggested by the manufacturer (Willy A. Bachofen Machinenfabrik, Switzerland). A homogeneous distribution of the NIF and the excipients was achieved by this mixing method without kneading or hard mechanical effects.

**Table 1. Ratio of the Niflumic Acid (NIF) and the Additives in the Samples Based on Weight**

| product | NIF | mannitol | poloxamer |
|---|---|---|---|
| conventional NIF | 1 | | |
| conventional NIF with excipients | 1 | 2.5 | 0.25 |
| submicrometer-sized NIF | 1 | | |
| submicrometer-sized NIF with excipients | 1 | 2.5 | 0.25 |

## RESULTS AND DISCUSSION

First, the plasma crystallization process is described, and its parameters are investigated for producing the desired products at a low temperature. Next, the produced NIF and Poloxamer 188 particles are characterized and their dissolution profiles are determined.

**Plasma Crystallization.** SDBD plasma crystallization is a new process for drug synthesis in the submicrometer size range. Plasma is an ionized gas that consists of electrons, ions, and neutral species, which are in an excited or ground state.[28] In the SDBD plasma, a large number of filamentary discharges (microdischarges) is produced. These microdischarges can ionize, for instance, aerosol droplets and dissociate them into smaller droplets or functionalize the surface of materials by adding or removing chemical groups without changing the bulk properties or appearance.[29]

During plasma crystallization, solution droplets, created by a nebulizer, are sprayed into the plasma. The plasma has two functions. First, the plasma acts as a heat source and, thus, enhances the evaporation rate of the solvent droplets. Second, the plasma electrically charges the solution droplets. As the surface charge of a droplet reaches a critical value (Rayleigh-limit), electrostatic forces overcome the surface tension and the droplet disrupts into a myriad of smaller droplets to reduce the surface charge density by creating more droplet surface area.[30] This disruption process is called Coulomb fission and results in micrometer-sized droplets of solution.[31]

Upon solvent evaporation, supersaturation for crystallization is created in the solution droplets.[32] At some point the driving force for crystallization becomes sufficiently large for crystal nucleation and growth to occur. At sufficiently low concentrations, nucleation of the dissolved organic compound will only start after the formation of the micrometer-sized solution droplets. Nano- or submicrometer-sized crystals will then be formed upon evaporation of all solvent from the micrometer-sized droplets. Figure 3 shows the schematics of the process.

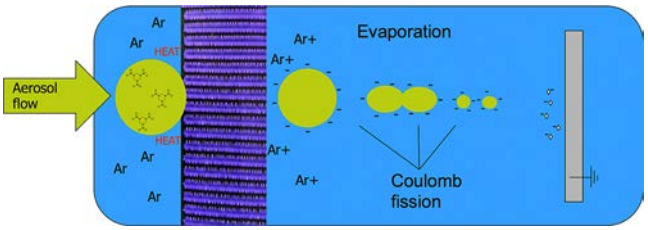


**Figure 3.** Process scheme of plasma aided crystallization. The NIF–acetone aerosol is carried by argon gas above the SDBD plate and interacts with the plasma. The plasma heats and charges the droplets, which results in enhanced evaporation of the solvent and Coulomb-fission of the droplets. At some point, the driving force for crystallization becomes sufficiently large for crystal nucleation and growth to occur. After the solvent is evaporated completely, the charged crystals are collected on the grounded reactor wall, where they lose their surface charge.

By applying a DC bias voltage superposed on the AC voltage, coalescence of the droplets is avoided while the particles can be collected on a specific location (Figure 3). By applying the DC bias, the charging effect of the droplets within the process is enhanced as described in a patent by Gundlach.[33] By this method, coalescence of the droplets and aggregation of the formed crystals is prevented because of their unipolar charges. Furthermore, by the application of the DC bias voltage, the charged crystals can be collected electrostatically with high efficiency using a grounded collector plate,[34] where they lose their surface charge.

**Plasma Process Parameters.** Table 2 shows the process parameters used for submicrometer-sized NIF production.

**Table 2. Process Parameters for the Reference Plasma Crystallization Experiment for NIF[a]**

| $\Delta U$ (kV) | $\Delta U_{bias}$ (kV) | $c$ (mg mL$^{-1}$) | $f$ (kHz) | $\varphi$ (L m$^{-1}$) |
|---|---|---|---|---|
| 3.7 | +2 | 20 | 10 | 11 |

[a]AC peak-to-peak potential difference ($\Delta U$), DC bias potential difference ($\Delta U_{bias}$), solution concentration ($c$), frequency ($f$), and argon gas flow rate ($\varphi$). Using these parameters, a homogeneous surface plasma is formed on the SDBD plate.

Using a solution concentration of 20 mg mL$^{-1}$ NIF in acetone, an argon flow rate of 11 L min$^{-1}$, a 10 kHz pulse excitation over the 3.7 kV potential difference, and a DC bias voltage of +2 kV, submicrometer-sized NIF crystals were produced. The 11 L min$^{-1}$ argon flow rate through the microchannels of the nebulizer results in approximately 4.5 mL min$^{-1}$ solution sprayed into the plasma reactor chamber when a solution concentration of 20 mg mL$^{-1}$ NIF in acetone is used.

**Plasma Temperature.** Figure 4 shows how the temperature profile developed 8 mm above the center of the SDBD plate during the plasma crystallization process. The average temperature above the SDBD plasma increased rapidly until 42 °C. Then the temperature decreased to around 40 °C and became stationary at that temperature. The temperature at the plate surface might be higher.

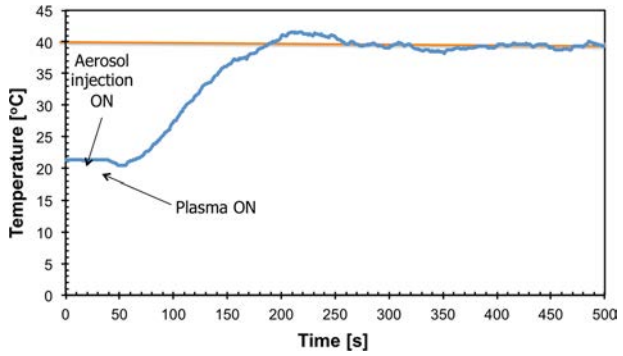


**Figure 4.** Temperature profiles measured 8 mm above the plasma surface. A stationary temperature around 40 °C was present during the submicrometer-sized particle generation.

**Product Characterization.** The produced NIF crystals are somewhat spherical, with a mean size of 700 nm (Figure 5).

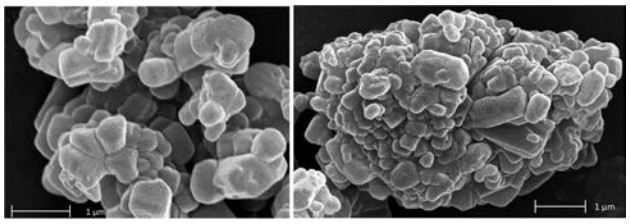

**Figure 5.** Left: NIF crystals in the size range 400−1000 nm. Right: A 6 μm aggregate of the submicrometer NIF crystals.

The submicrometer-sized NIF crystals are aggregated into 5−6 μm sized clusters, which can be seen by the clearly visible border lines of the individual NIF crystals. The submicrometer NIF crystals possibly stick together due to the strong interactions between the hydrophobic crystal surfaces or due to static charging of these small crystals.

**Excipient.** Poloxamer 188 was also produced by plasma crystallization, with the same process parameters used for NIF (Table 2). The product is from spherical to irregular shape in the size range 1−3 μm (Figure 6), which is larger than the NIF made by plasma crystallization. Poloxamer 188 formed a large amount of irregular shaped large crystals that are probably agglomerates. A possible explanation for the relatively large size and tendency for agglomeration can be the semicrystalline nature and the macromolecular structure of the Poloxamer 188, which leads to a viscous solution. In case the initial solution is highly viscous in the plasma crystallization process, the product is generally larger, and agglomerates can be present.

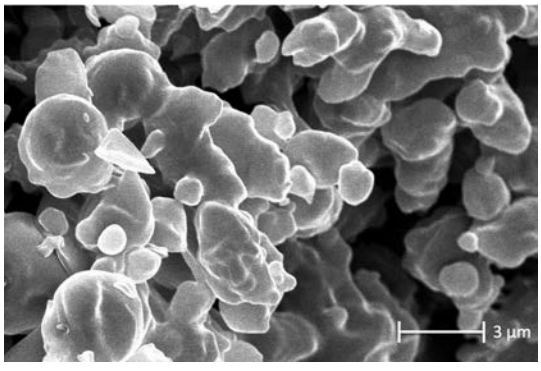


**Figure 6.** 200−800 Poloxamer 188 in the micrometer size range produced by cold plasma technology.

**Solid State Analysis (DSC, XRD, FT-IR).** The structural characterizations were performed to check the crystallinity of the produced NIF crystals and Poloxamer 188. The melting point of the submicrometer-sized NIF was measured to be 202.9 °C, slightly lower than that of the original material (203.4 °C) and than the literature values[19] (see Figure S2 in the Supporting Information). The lower melting point could be explained by the relatively large surface area and, thus, increased total surface free energy compared to the case of the original material.[35] Poloxamer is a semicyrstalline material with a melting point around 56 °C. Its melting point decreased slightly to 53.6 °C (see Figure S2 in the Supporting Information), probably again due to the size reduction and thus increased total surface free energy of the material.

There is a relation between the crystallinity and normalized heat of melting of the samples.[36] The DSC results show that the normalized heat of melting for the submicrometer-sized NIF was 113.6 J $g^{-1}$, 80% of that for the conventional NIF (140.4 J $g^{-1}$). This indicates that the plasma-made NIF is 80% crystalline and 20% amorphous. The heat of melting for the plasma-made Poloxamer 188 is 93% of that for the conventional material, indicating a 7% decrease in crystallinity due to the plasma process.

The XRPD patterns of the submicrometer-sized NIF crystals showed the single known crystal form for both NIF[37] and Poloxamer 188[38] (see Figure S3 in the Supporting Information).

FT-IR spectroscopy was performed to investigate the possible changes in the molecular structure. The IR spectra showed that both the produced NIF and Poloxamer 188 did not alter chemically in the process, since no physical transition or decomposition was observed (see Figure S4 in the Supporting Information).

**Dissolution Rate Measurements.** Dissolution rate measurements were performed at gastric pH (pH 1.2). While the conventional NIF has a low dissolution rate (31% of the drug dissolving in the first hour), that of the conventional NIF in the presence of the conventional excipients D-mannitol and Poloxamer 188 is already somewhat higher, with 40% of the drug dissolving in the first hour (Figure 7). The submicrometer-sized NIF without the excipients had a slightly higher dissolution rate, with around 50% dissolving in one hour. Interestingly, by mixing the conventional NIF with the plasma-made Poloxamer 188 and conventional D-mannitol, the dissolution rate increased significantly: 81% of the NIF was dissolved within one hour due to the increased efficiency of the plasma-made Poloxamer 188. The dissolution rate further increased upon using the submicrometer-sized NIF with the plasma-made Poloxamer 188 and conventional D-mannitol: 76% of NIF was already dissolved after 15 min while as much as 96% was dissolved in one hour. Within 90 min the NIF was completely dissolved.

In general, the excipient, Poloxamer 188, deaggregates and increases the wettability of the NIF crystals, which helps the dissolution behavior of the NIF crystals.[39,40] Apparently, the Poloxamer 188 helps the dissolution of the hydrophobic NIF crystals more efficiently when its size is reduced. Via size reduction, significantly higher surface area can be achieved that leads to an increased interaction between the drug and excipient sites, which results in more efficient deaggregation of the NIF.


dx.doi.org/10.1021/cg301026b | Cryst. Growth Des. 2012, 12, 5090−5095

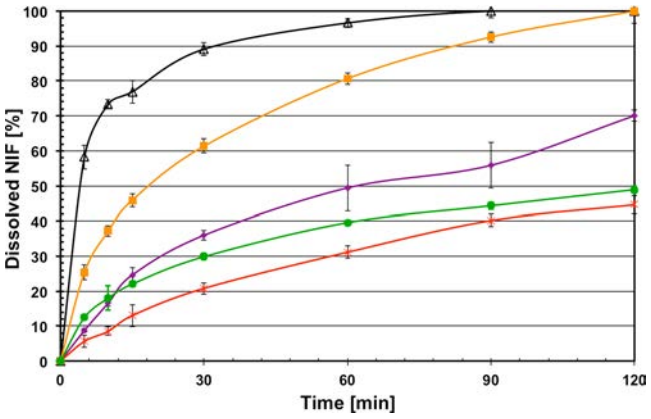


**Figure 7.** Dissolution profiles of the conventional NIF and the submicrometer NIF with and without the excipient D-mannitol and Poloxamer 188 at pH 1.2. Only 20% of the conventional NIF (red times signs) was dissolved into the solution after 30 min. Using the conventional NIF with the conventionally sized excipients (green circles), 30% of the drug was dissolved after 30 min. The dissolution of the submicrometer-NIF (purple diamonds) was slightly higher; 36% of the drug was dissolved in the same time. By adding the plasma-made Poloxamer 188 and conventional D-mannitol to the conventional NIF (orange boxes), 61% of the drug was dissolved in 30 min. When the submicrometer-sized NIF was applied with the plasma-made Poloxamer 188 and conventional D-mannitol (black triangles), the dissolution increased to 89% after 30 min.

When the micrometer-sized, plasma-made Poloxamer 188 is used with the submicrometer NIF, it can very rapidly and effectively disintegrate the aggregated NIF clusters, and due to the extremely high surface area of NIF crystals, rapid dissolution can occur. Thus, preparation of submicrometer-sized NIF and few micrometer-sized Poloxamer 188 can result in substantially higher drug liberation and absorption than can be achieved by the conventional compounds. The synergy between the aggregation prevention of the excipients and the increased surface area of the submicrometer-sized NIF results in a substantially increased dissolution rate of NIF.

## CONCLUSIONS

Via the size reduction of the drug particles and/or excipient particles, it is possible to enhance the dissolution profile of poorly soluble active pharmaceutical ingredients and therefore increase their bioavailability. Submicrometer-sized niflumic acid crystals with a mean size of 700 nm were produced by atmospheric pressure cold plasma crystallization. The submicrometer crystals aggregated into 5−6 $\mu$m particle clusters due to the large specific surface area and/or static energy of the crystals. The product was highly crystalline and had a slightly lower melting point than the conventional niflumic acid. Its commonly used excipient, Poloxamer 188 in the size range of 1−3 $\mu$m, was also produced by atmospheric pressure cold plasma crystallization. Agglomeration of the Poloxamer 188 particles was observed, which was probably due to its macromolecular structure and semicrystalline nature. Dissolution rate measurements showed that using the produced few micrometer-sized Poloxamer 188 with the conventional niflumic acid already leads to a substantial increase in the dissolution rate. When the plasma-made Poloxamer 188 was applied with the produced submicrometer-sized niflumic acid crystals, the dissolution rate increased even more and the niflumic acid dissolved completely within 90 min. Atmospheric pressure cold plasma crystallization is an interesting crystallization technique that leads to submicrometer particles that can have significantly improved properties such as dissolution rate.

## ASSOCIATED CONTENT

### Supporting Information

SEM image of the niflumic acid crystals, obtained from the manufacturer, DSC spectra of the submicrometer-sized niflumic acid and of the plasma-made Poloxamer 188 compared to the original samples, XRD patterns of the submicrometer-sized niflumic acid and of the plasma-made Poloxamer 188 compared to the conventional ones, and FT-IR spectra of the submicrometer-sized niflumic acid and of the plasma-made Poloxamer 188 compared to the original samples. This material is available free of charge via the Internet at http://pubs.acs.org.

## AUTHOR INFORMATION

### Corresponding Author

*E-mail: kefehu@gmail.com.

### Notes

The authors declare no competing financial interest.

## ACKNOWLEDGMENTS

The authors thank Yves Creyghton for the introduction to plasma crystallization and for providing the laboratory and equipment. Furthermore, the authors also thank Willem Duvalois and Emile van Veldhoven for the sample analysis, and Marcel Simor for interesting and helpful discussions. "TÁMOP-4.2.1/B-09/1/KONV-2010-0005. Creating the Center of Excellence at the University of Szeged" is supported by the European Union and cofinanced by the European Regional Development Fund.

## REFERENCES

(1) *Handbook of Industrial Crystallization*; Myerson, A. S., Ed.; Butterworth-Heinemann Ltd.: Oxford, 1993.
(2) Babu, N. J.; Nangia, A. *Cryst. Growth Des.* **2011**, *11*, 2662−2679.
(3) Patil, M. P.; Pandit, A. B. *Ultrasonics Sonochem.* **2007**, *14*, 519−530.
(4) Leuner, C.; Dressmann, J. *Eur. J. Pharm. Biopharm.* **2000**, *50*, 47−60.
(5) Rabinow, B. E. *Nat. Rev. Drug Discovery* **2004**, *3*, 785−796.
(6) Kata, M.; Ambrus., R.; Aigner, Z. *J. Inclusion Phenom.* **2002**, *44*, 123−126.
(7) Kesisoglou, F.; Panmai, S.; Wu, Y. *Adv. Drug Delivery Rev.* **2007**, *59*, 631−644.
(8) Müller, R. H.; Peters, K. *Int. J. Pharm.* **1998**, *160*, 229−237.
(9) Liversidge, G. G.; Conzentino, P. *Int. J. Pharm.* **1995**, *125*, 309−313.
(10) Trotta, M.; Gallarete, M.; Pattarino, F.; Morel, S. *J. Controlled Release* **2001**, *76*, 119−128.
(11) Peters, K.; Leitzke, S.; Diederichs, J. E.; Borner, K.; Hahn, H.; Müller, R. H.; Ehlers, S. *J. Antimicrob. Chem.* **2000**, *45*, 77−83.
(12) Hecq, J.; Deleers, M.; Fanara, D.; Vranckx, H.; Amighi, K. *Int. J. Pharm.* **2005**, *299*, 167−177.
(13) Debuigne, F.; Cuisenaire, J.; Jeunieau, L.; Masereel, B.; Nagy, J. B. *J. Colloid Interface Sci.* **2001**, *243*, 90−101.
(14) Suryanarayana, C. *Prog. Mater. Sci.* **2001**, *46*, 1−184.
(15) Radacsi, N.; Ambrus, R.; Szunyogh, T.; Szabó-Révész, P.; Stankiewicz, A. I.; van der Heijden, A. E. D. M.; ter Horst, J. H. *Cryst. Growth Des.* **2012**, *12*, 3514−3520.
(16) Simor, M.; Fiala, A.; Kovacik, D.; Hlidek, P.; Wypkema, A.; Kuipers, R. *Surf. Coat. Technol.* **2007**, *201*, 7802.

(17) Vons, V.; Creyghton, Y. L. M.; Schmidt-Ott, A. *J. Nanopart. Res.* **2006**, *8*, 721−728.
(18) Carneiro, N.; Souto, A. P.; Silva, E.; Marimba, A.; Tena, B.; Ferreira, H.; Magalhaes, V. *Color. Technol.* **2001**, *117*, 298.
(19) *The Merck Index*, 11th ed.; Budavari, S., O'Neil, M. J., Smith, A., Heckelman, P. E., Eds.; Merck & Co.: Rahway, NJ, 1989; Monograph 6444.
(20) *Martindale: The Extra Pharmacopoeia*, 31st ed.; Reynolds, J. E. F., Ed.; The Royal Pharmaceutical Society: London, 1996.
(21) Takács-Novák, K.; Avdeef, A.; Box, K. J.; Podányi, B.; Szász, Gy. *J. Pharm. Biomed. Anal.* **1994**, *12*, 1369−1377.
(22) Ambrus, R.; Aigner, Z.; Dehelean, C.; Szabó-Révész, P. *Rev. Chim.* **2007**, *58*, 60−64.
(23) Salge, J. *Surf. Coat. Technol.* **1996**, *80*, 1−7.
(24) Abramoff, M. D.; Magelhaes, P. J.; Ram, S. J. *Biophotonics Int.* **2004**, *11/7*, 36−42.
(25) Remias, R.; Kukovecz, Á.; Daranyi, M.; Kozma, G.; Varga, S.; Kónya, Z.; Kiricsi, I. *Eur. J. Inorg. Chem.* **2009**, *24*, 3622−3627.
(26) *European Pharmacopoeia*, 3rd ed.; Council of Europe: Strasbourg, 1996; pp 128−129.
(27) Aronson, J. K. In *Meyler's Side Effects of Drugs: The international Encyclopedia of Adverse Drug Reactions and Interactions*, 15th ed.; Elsevier: Oxford, 2006; pp 2203−2204.
(28) Eliasson, B.; Kogelschatz, U. *IEEE Trans. Plasma Sci.* **1991**, *19*, 1063−1077.
(29) Rahel, J.; Simor, M.; Cernak, M.; Stefecka, M.; Imahori, Y.; Kando, M. *Surf. Coat. Technol.* **2003**, *169*, 604−608.
(30) Rayleigh, L. *Philos. Mag.* **1882**, *14*, 184−186.
(31) Suzuki, K.; Matsumoto, H.; Minagawa, M.; Kimura, M.; Tanioka, A. *Polym. J.* **2007**, *39*, 1128−1134.
(32) Mullin, J. W. *Crystallization*, 4th ed.; Butterworth-Heinemann Ltd.: Oxford, 2001.
(33) Gundlach, R. W. *DC biased AC corona charging*. U.S. Patent 6,349,024, February 19, 2002.
(34) Rhodes, M. *Introduction to Particle Technology*, 2nd ed.; West Sussex: John Wiley & Sons Ltd., 2008.
(35) Yang, G. C.; Nie, F. D.; Huang, H. *J. Energy Mater.* **2007**, *25*, 35−47.
(36) Wagner, M. *Thermal analysis in practice*; Mettler-Toledo AG: Schwerzenbach, 2009; Chapter 7.6: DSC Evaluations, pp 90−132.
(37) Krishna Murthy, H. M.; Vijayan, M. *Acta Crystallogr.* **1979**, *B35*, 262−263.
(38) Sharma, A.; Jain, C. P. *Pharm. Lett.* **2010**, *2*, 54−63.
(39) Ghosh, I.; Bose, S.; Vippagunta, R.; Harmon, F. *Int. J. Pharm.* **2011**, *409*, 260−268.
(40) Myers, D. *Surfaces, Interfaces and Colloids: Principles and Applications*, 2nd ed.; Wiley-VCH: Weinheim, 1999.